Nonlinear Climate Responses to Changes in Antarctic Intermediate Water

JENNIFER A. GRAHAM

School of Environmental Sciences, University of East Anglia, Norwich, United Kingdom

DAVID P. STEVENS

School of Mathematics, University of East Anglia, Norwich, United Kingdom

KAREN J. HEYWOOD

School of Environmental Sciences, University of East Anglia, Norwich, United Kingdom

(Manuscript received 25 October 2012, in final form 11 June 2013)

ABSTRACT

The global impact of changes in Antarctic Intermediate Water (AAIW) properties is demonstrated using idealized perturbation experiments in a coupled climate model. Properties of AAIW were altered between 10° and 20°S in the Atlantic, Pacific, and Indian Oceans separately. Potential temperature was changed by ±1°C, along with density-compensating changes in salinity. For each of the experiments, sea surface temperature responds to changes in AAIW when anomalies surface at higher latitudes (>30°). Anomalous sea-to-air heat fluxes leave density anomalies in the ocean, resulting in nonlinear responses to opposite-sign perturbations. In the Southern Ocean, these affect the meridional density gradient, leading to changes in Antarctic Circumpolar Current transport. The response to cooler, fresher AAIW is both greater in magnitude and significant over a larger area than that for warmer, saltier AAIW. The North Atlantic is particularly sensitive to cool, fresh perturbations, with density anomalies causing reductions in the meridional overturning circulation of up to 1 Sv (1 Sv $\equiv 10^6\,m^3\,s^{-1}$). Resultant changes in meridional ocean heat transport, along with surfacing anomalies, cause basinwide changes in the surface ocean and overlying atmosphere on multidecadal time scales.

1. Introduction

Antarctic Intermediate Water (AAIW) is formed in the Southern Ocean, north of the Subantarctic Front. From here, it flows northward in each of the three major ocean basins, at intermediate depths (~1000 m), becoming the most widespread of all the intermediate water masses (Hanawa and Talley 2001). AAIW can be identified as a subsurface salinity minimum, accompanied by low temperatures. Early studies suggested that this water mass formed through a combination of deep winter convection and cross-frontal exchange of Antarctic Surface Water (e.g., McCartney 1977; Molinelli 1981; Piola and Gordon 1989). The relative importance of the various mechanisms in determining the formation and variability of AAIW properties is still uncertain. Talley (1996) cited the importance of mixing in the southwestern Atlantic. The role of eddies in the mixing process has also been strongly recognized in a number of further studies (e.g., Marshall 1997; Sloyan et al. 2010). Santoso and England (2004) suggested that meltwater fluxes around the Antarctic continent were important in a circumpolar formation process, along with surface heat and freshwater fluxes. Other studies have shown that wind forcing, leading to cross-frontal Ekman transport, plays a key role (Oke and England 2004). However, it is believed that on longer (decadal) time scales, the role of surface fluxes is likely to be more important (Downes et al. 2010).

Recent observations suggest that the temperature and salinity of AAIW have changed (e.g., Aoki et al. 2005; Naveira Garabato et al. 2009; Helm et al. 2010; Schmidtko and Johnson 2012). Aoki et al. (2005) used a series of cruise sections, between the 1950s and 1990s, to show that there has been a cooling and freshening

Corresponding author address: Jennifer A. Graham, Center for Coastal Physical Oceanography, Old Dominion University, 4111 Monarch Way, Norfolk, VA 23508.
E-mail: jgraham@ccpo.odu.edu

DOI: 10.1175/JCLI-D-12-00767.1

on density surfaces above the core of AAIW in the Pacific and Indian sectors of the Southern Ocean. Salinity changes are shown to be on the order of 0.02, and temperature changes around −0.2°C. Such signals have been attributed to warming surface waters and an increased hydrological cycle, both signatures of anthropogenic climate change (Banks and Bindoff 2003; Helm et al. 2010). Helm et al. (2010) have used a combination of ship-based observations and Argo profiles to show that between 1970 and 2005 there has been a global average decline in salinity on AAIW density surfaces, equating to a 16% increase in precipitation minus evaporation over the Southern Ocean. The mean decline in Atlantic AAIW salinity was shown to be 0.04 ± 0.04. Naveira Garabato et al. (2009) used a series of 24 repeat transects through Drake Passage, between 1969 and 2005, to show that AAIW had freshened by about 0.05. This was likely caused by both increased precipitation and a retreating winter sea ice edge to the west of the Antarctic Peninsula. This has been attributed to the positive trend in the southern annular mode (SAM), which has occurred since the 1970s. More recently, Schmidtko and Johnson (2012) have used observations since the 1920s to show that the salinity minimum has warmed and shoaled, with a decreased density. However, contrary to Helm et al. (2010), they show little change in salinity at the AAIW core, with trends varying regionally. Schmidtko and Johnson (2012) also show that the SAM alone cannot be responsible for recent changes observed in AAIW.

Although the observational evidence so far appears conflicting, climate projections show that the properties of AAIW are likely to change in the future, as surface heat and freshwater fluxes change in the formation regions (e.g., Wong et al. 1999; Bindoff and McDougall 2000; Sen Gupta et al. 2009; Downes et al. 2010). Sen Gupta et al. (2009) show a projected warming throughout intermediate depths in the Southern Hemisphere, of up to 1°C, over the next century. Their projections of salinity changes are less consistent between basins but suggest a decreased salinity in the upper 1000 m, and increased salinity at greater depth between 60° and 40°S. Downes et al. (2010) show that changes in surface heat and freshwater fluxes in the formation regions lead to a warming and freshening of AAIW by 2100, during the Intergovernmental Panel on Climate Change (IPCC) A2 emissions scenario (where atmospheric CO_2 reaches 860 ppm at 2100). The rate of subduction also decreases because of increased buoyancy and decreased mixed-layer depths in these regions. As the water mass moves to lower densities, a cooling and freshening is observed on isopycnals lighter than that of the previous salinity minimum (Downes et al. 2010).

While previous work has focused predominantly on how AAIW may change, there has been little investigation into how such changes may feed back onto the climate system. AAIW is known to be a fundamental part of the global ocean circulation, and hence of the global climate system. Any changes to this water mass are then likely to have consequences for other aspects of the climate system. Understanding these potential feedbacks is crucial for improving predictions of how our climate may change in the future. Graham et al. (2011, hereafter referred to as G11) showed that cooling and freshening of AAIW in the South Atlantic can lead to a significant cooling in the surface North Atlantic and a reduction of the meridional overturning circulation (MOC) on multidecadal time scales. The ensemble setup used by G11 used the same initial ocean conditions for each ensemble member, varying only initial conditions in the atmosphere. Therefore, it is possible that those results may be influenced by the initial ocean state, which may predispose the climate system to react in a particular way. Here, we use an ensemble setup with varying initial conditions in both the ocean and atmosphere. These experiments can then reveal the response to varying AAIW, irrespective of the ocean initial conditions. Experiments have also been extended to the Pacific and Indian Oceans, allowing the first insight into responses to AAIW changes on a global scale.

2. Methods

A series of six ensemble perturbation experiments was carried out using the coupled climate model HadCM3 (the third climate configuration of the Met Office Unified Model) (Gordon et al. 2000). The ocean component of HadCM3 has a resolution of 1.25° × 1.25°, and 20 vertical levels. The atmosphere component has a resolution of 2.5° × 3.75°, and 19 vertical levels. In general, HadCM3 performs well, reproducing a salinity minimum at intermediate depths in each of the three major ocean basins (Fig. 1). The water mass is fresher and lighter than observed (and hence found at shallower depths in the model than observed), likely because of an increased hydrological cycle in the model (Sloyan and Kamenkovich 2007; Pardaens et al. 2003). However, as we are performing idealized perturbations, to compare with a control simulation, HadCM3 is a useful tool for this study. The internal climate variability compares well with observations (Collins et al. 2001).

Properties of AAIW in HadCM3 were altered between 10° and 20°S in each ocean basin separately, far removed from the water mass formation and subduction regions (Fig. 1). This latitude band was chosen since AAIW is clearly visible in the water column, with

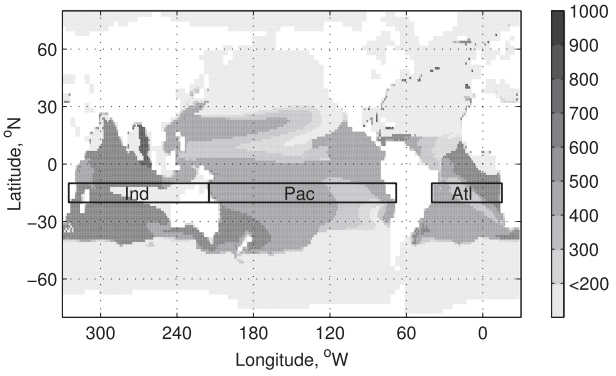

FIG. 1. Depth (m) of subsurface salinity minimum in HadCM3 (depth 200–1000 m). If no salinity minimum is found between 200 and 1000 m, depth is shown as <200 m. Boxes show the perturbed regions in the Atlantic, Pacific, and Indian Oceans, 10°–20°S.

a salinity minimum found beneath the surface thermocline. Perturbing at this latitude allows us to focus on the impact of AAIW on the surface waters and climate as it moves northward in each of the major ocean basins. Performing a separate experiment for each ocean basin allows us to distinguish the relative influence of each basin's intermediate water on the climate system. This is important in the context of planning future observations and also since both climate projections and recent observations suggest that future changes in AAIW may not necessarily be the same in each basin (e.g., Sen Gupta et al. 2009; Schmidtko and Johnson 2012).

For each ocean, two experiments were carried out, varying temperature by +1°C (Atl+, Pac+, and Ind+) and −1°C (Atl−, Pac−, and Ind−). A density-compensating change in salinity was also made to allow AAIW to initially follow its usual path of circulation. This gave an average salinity change of ±0.2. By eliminating dynamical impacts in the perturbation, we can see how AAIW affects the surface regions as it follows its usual paths of circulation. Experimental setup follows the methods described by G11, with the temperature perturbations performed between AAIW density boundaries for each of the relevant basins, chosen to encompass the salinity minimum at depth. Figure 2 shows these density boundaries, chosen as 27.9–29.4 for the Atlantic, 27.2–29.1 for the Pacific, and 27.5–29.1 for the Indian Ocean, calculated relative to the mean depth of the salinity minimum (447–666 m, level 11 in HadCM3). A perturbation of ±0.5°C, along with the corresponding salinity change, was also made in the model levels directly above and below these boundaries, allowing for a smoother transition in the water column (Fig. 2).

The chosen perturbations are much larger than the internal variability of AAIW in HadCM3. The magnitude of these imposed changes is also much larger than

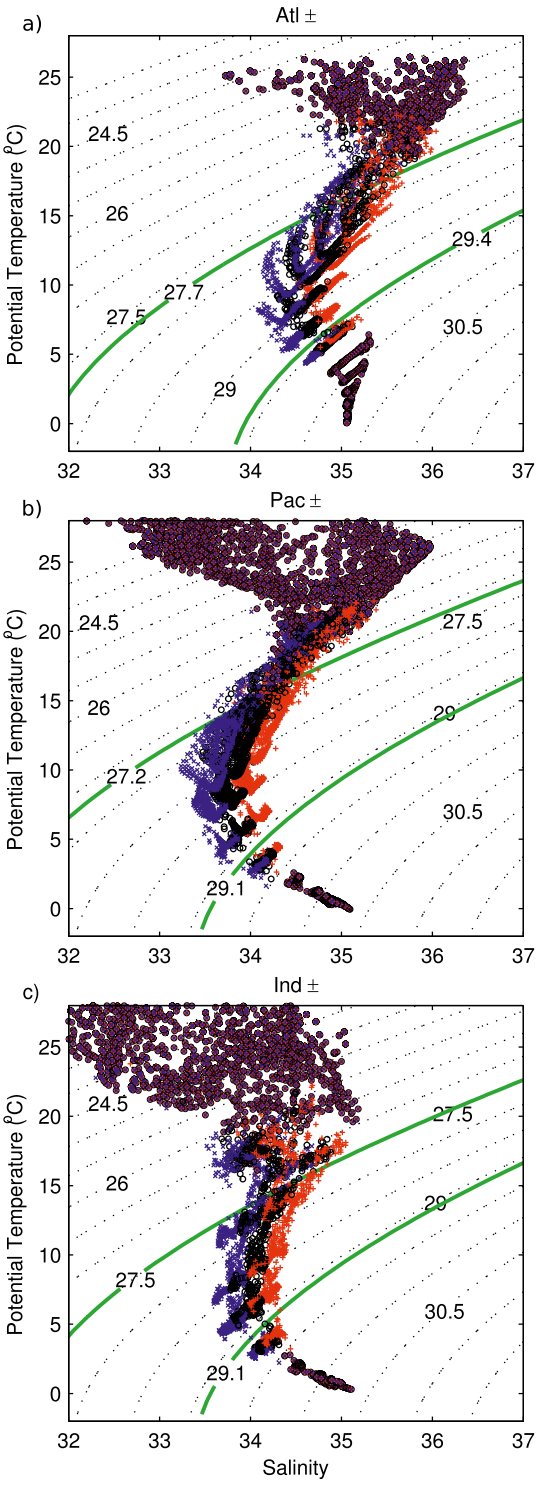

FIG. 2. Potential temperature–salinity plot for perturbation and control start dumps, 10°–20°S, in the (a) Atlantic (Atl±), (b) Pacific (Pac±), and (c) Indian (Ind±) Oceans. Blue crosses and red plus signs show the conditions for the −1° and +1°C perturbations, respectively. Black circles show the control conditions. Black contours show the corresponding potential density values, calculated relative to a depth of about 500 m. Green contours show the chosen boundaries of AAIW for each basin.

those observed (e.g., Helm et al. 2010; Aoki et al. 2005). While a substantial change is made to the heat and salt content of AAIW, choosing a perturbation of ±1°C maintains the characteristic salinity minimum during the density-compensating warming perturbation. It is worth remembering that the key aim of this study is to understand the processes involved and not to make predictions of the magnitude of future changes. However, as Sen Gupta et al. (2009) show a temperature change of +1°C and a freshening of 0.1 in regions of AAIW formation by the end of the twenty-first century, this magnitude of temperature perturbation may not be far outside the projected changes in AAIW over centennial time scales, although our salinity perturbation is much larger.

All of the nine member ensembles were integrated for 100 years, with initial conditions for each experiment being identical to those in the control ensemble, aside from the perturbations in the relevant ocean basin. Previous ensemble experiments, discussed in G11, used the same initial ocean conditions, but different initial atmosphere conditions, separated by 1 day. While the variation in atmospheric conditions does impose a variety of responses, it is possible that initial conditions in the ocean may predispose the model to react in a particular way. To address this issue, each ensemble member in this study has variations in both the ocean and atmosphere initial conditions, with inputs taken from a 500-yr control run. Taking the start date of the first ensemble member as year 0, the additional ensemble members then start at years 50, 100, 150, . . . , 400 (each separated by 50 years). For each starting point, both the control ocean and atmosphere will then behave differently over the following 100-yr integration. These ensemble experiments show how the perturbation affects the climate, irrespective of the ocean initial conditions. The results discussed in the following section will all refer to ensemble means of each experiment. Hereafter, the term significant is used to describe results that are statistically significant at the 95% confidence level, determined using a paired *t* test.

3. Results

a. Surfacing anomalies

Heat and salt spread by advection and diffusion at equal rates in the model, along the same paths, maintaining approximately constant density. Changes arise when the water mass comes into contact with the atmosphere. Surfacing temperature anomalies can drive an atmospheric response, which can act to reduce the anomaly through anomalous atmosphere-to-ocean heat fluxes. However, there is no direct atmospheric response to surface salinity changes. Therefore, a salinity anomaly can be used as a tracer for the perturbed water mass, and if the anomaly extends from intermediate depths to the sea surface, this indicates where AAIW surfaces.

For each of these experiments, sea surface salinity (SSS) anomalies with the same sign as the initial perturbation can be found in equatorial regions (Figs. 3, 4, and 5). As the anomalous water mass is advected northward from the perturbed region, easterly winds lead to poleward Ekman transport and upwelling along the equator. This brings the upper portion of the perturbed water mass to the surface (Fig. 3). During years 1–50 of the experiment, the largest areas of significant anomalies are found in the Pacific, for both Pac+ and Pac− (Figs. 4c,d). Figure 6a shows the decadal-mean SSS anomalies for the Niño-3.4 index region (5°N–5°S, 170°–120°W), for each of the six experiments. Statistically significant anomalies occur for Pac+ and Pac−, with the decadal-mean SSS for Pac+ remaining above the range of the control ensemble for 100 years. For Pac−, the anomalies are outside the range of the control ensemble during the first 50 years, showing that AAIW reaches the surface in equatorial regions. There is also a response in the Niño-3.4 region for the other experiments. For Ind+, significant salinity anomalies are found in the Niño-3.4 region (Fig. 6a). However, as these anomalies are seen for years 1–10, they are more likely to be due to remote forcing, such as an atmospheric teleconnection, rather than advection of the anomalous water mass from the Indian Ocean. Along the eastern boundaries of ocean basins, prevailing winds can also lead to coastal upwelling. SSS anomalies can be found along the eastern boundaries of the Atlantic, Pacific, and Indian Oceans (Fig. 4). However, these anomalies are typically less persistent than those found in the equatorial Pacific (for Pac+) and are therefore less apparent during years 51–100 (Fig. 5). In the eastern boundary of the South Pacific, significant SSS anomalies are found during years 1–30 for Pac+ and years 1–10 for Pac−. Despite persistent SSS anomalies being found around the equator, there is no corresponding signal in sea surface temperature (SST; Figs. 6b and 7). For Pac+ and Pac−, there is evidence to suggest that more or less heat is being lost from the ocean to the atmosphere, respectively, when the perturbed water mass surfaces in the eastern tropical Pacific (Fig. 8). Unlike the anomalous salt content, the heat anomaly can be reduced through a direct atmospheric response. As it is lost to the atmosphere, the anomalous surface heat content is not sufficiently large to cause statistically significant changes in sea surface temperature when compared with the range of internal climate variability.

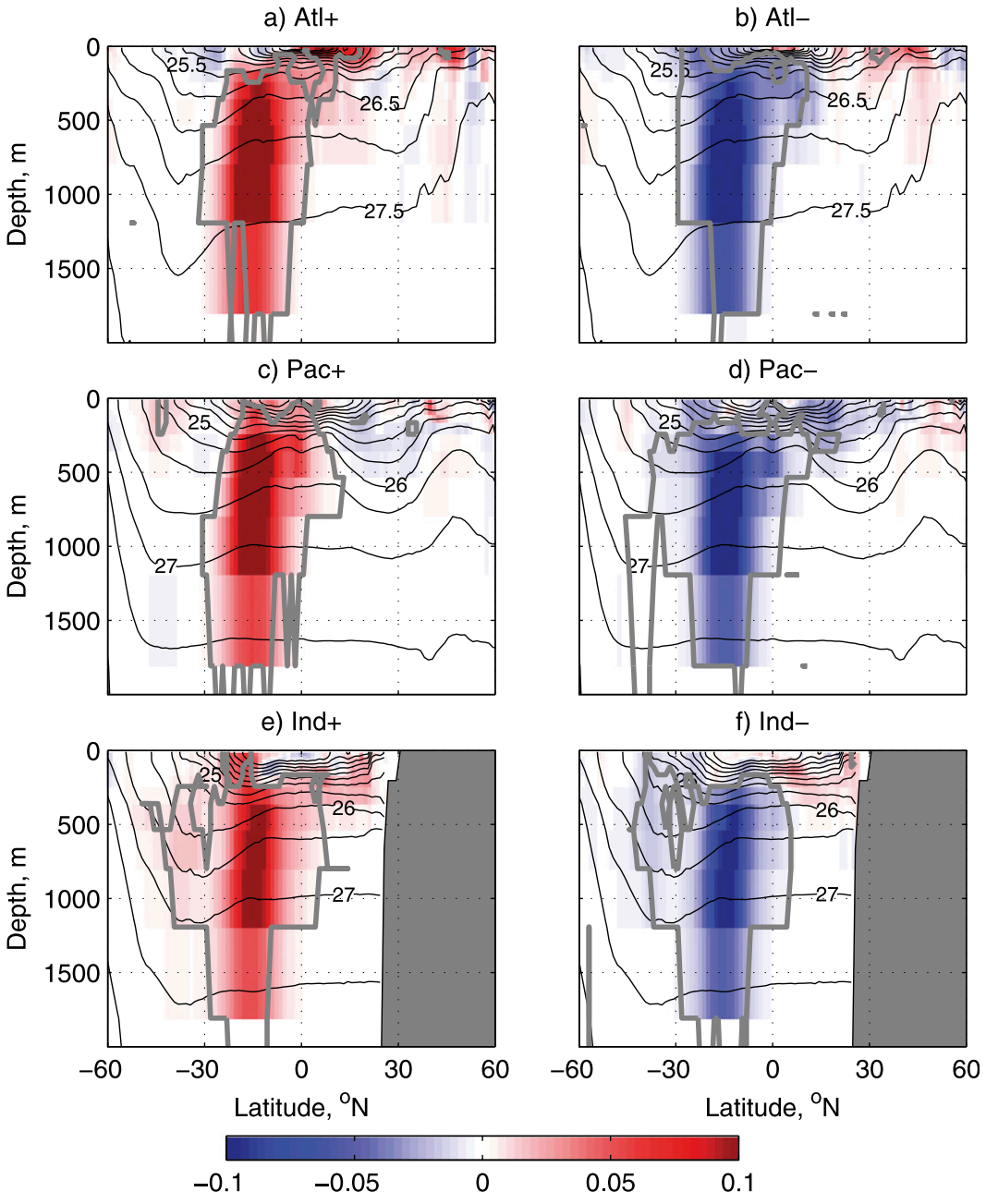

FIG. 3. Zonal average salinity anomalies for each experiment for years 1–10, with respect to the control ensemble mean for the same period. Black contours show control potential density conditions for years 1–10 relative to the surface level of HadCM3. Thick gray contours show regions where the anomalies are significant at the 95% confidence level.

As isopycnals shoal toward high latitudes, AAIW moves closer to the surface as it is advected northward in the North Atlantic and Pacific, or southward, into the Southern Ocean (Fig. 9). This, along with deeper mixed layers, brings the anomalous heat and salt content to the surface (Figs. 4, 5, and 7). For perturbations in the Atlantic, G11 show that the anomalous water mass moves northward and surfaces in the North Atlantic Current, subpolar gyre and Greenland, Iceland, and Norwegian Seas. In the subtropical North Atlantic and subpolar gyre, positive and negative anomalies in SSS can be found for Atl+ and Atl−, respectively (Figs. 4a,b). For Atl−, there are significant SSS anomalies in the North Atlantic during years 51–100 (Fig. 5b). Significant

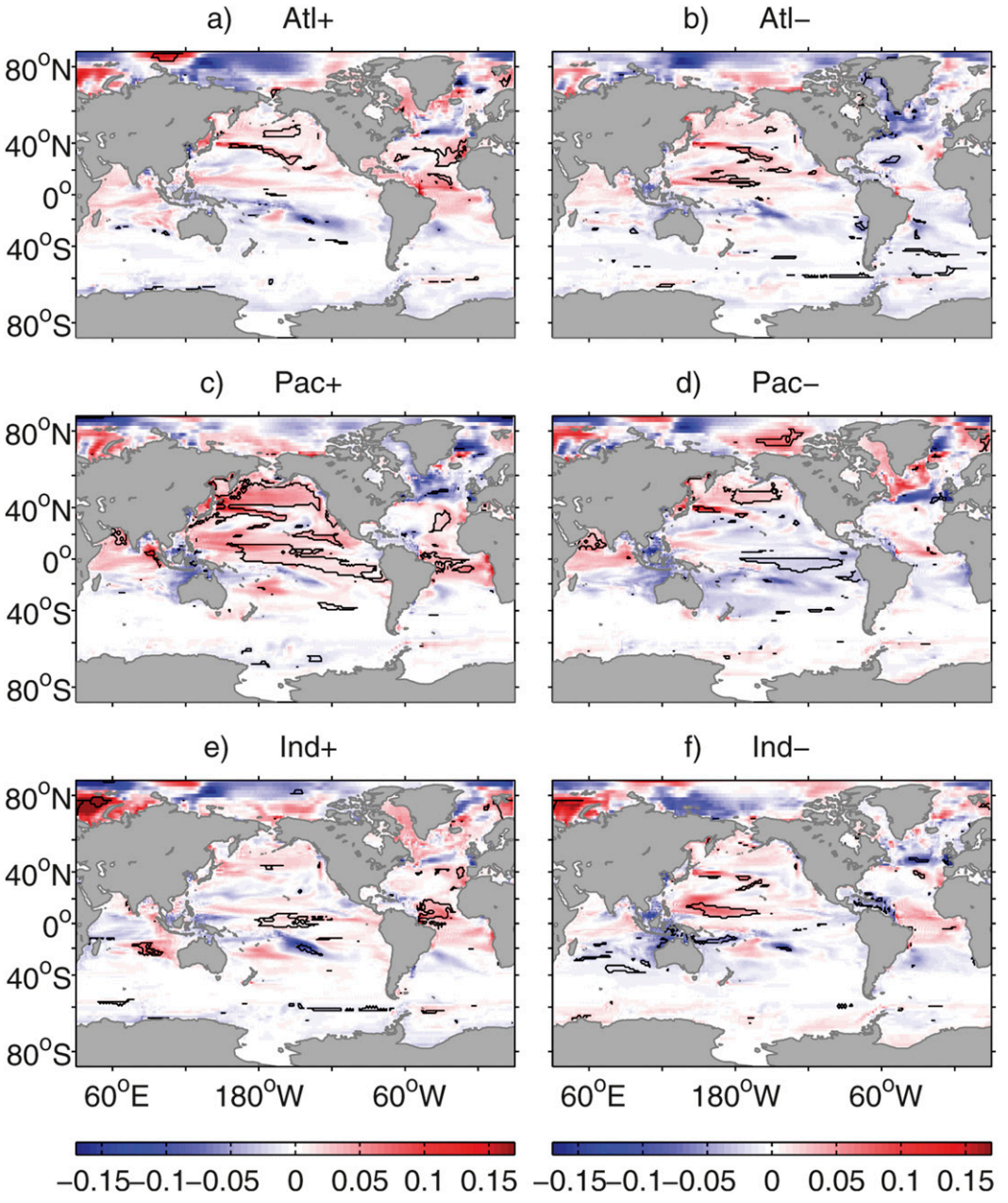

FIG. 4. Mean global SSS response to each experiment for years 1–50. Values shown are anomalies with respect to the control ensemble mean for years 1–50. Black contours indicate regions where the anomalies are significant at the 95% confidence level.

SSS anomalies occur during years 31–40 for Atl+. Salinity anomalies are also found in the subtropical Pacific for Pac+ and Pac− (Figs. 4c,d and 5c,d).

Salinity anomalies can reach the surface in the southern Indian Ocean (between approximately 15° and 45°S) during the first 10 years of the simulation (Figs. 3e,f). Unlike the Pacific and Atlantic Oceans, the Indian Ocean has a net southward transport of intermediate waters (~500–2000 m), out of the basin (You 1998). This allows a greater dispersion of the anomalous water mass throughout the global ocean, when compared with perturbations in the Atlantic and Pacific. For Ind−, there is a mean reduction in SSS between 30° and 50°S for 100 years (Figs. 4, 5 and 6c). This reduction is outside the range of the control ensemble mean for the majority of the simulation. For Ind+, there is an increased SSS for

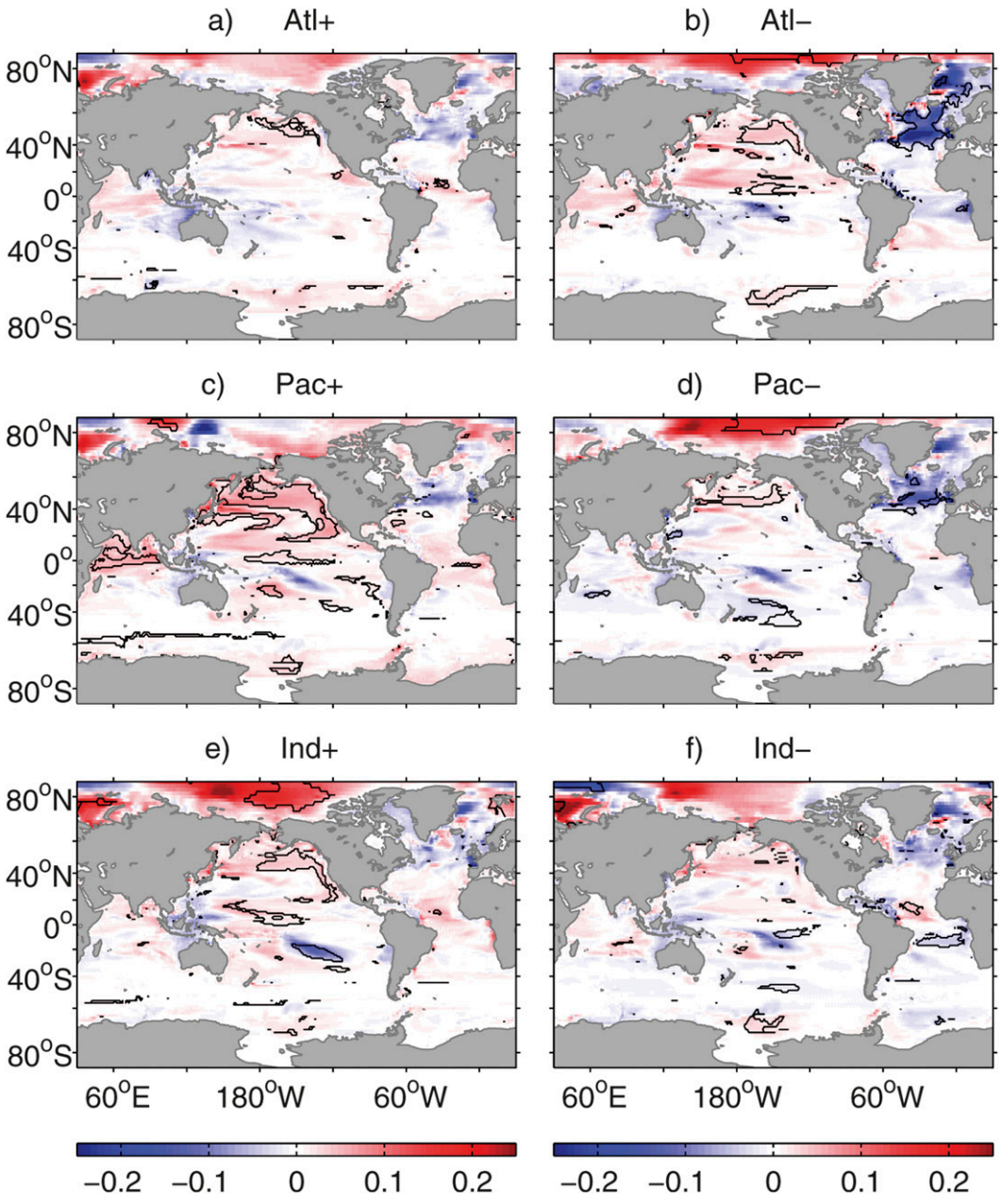

FIG. 5. Mean global SSS response to each experiment for years 51–100. Values shown are anomalies with respect to the control ensemble mean for years 51–100. Black contours indicate regions where the anomalies are significant at the 95% confidence level.

years 30–100. For Pac+, the mean SSS to the north of the Southern Ocean is actually reduced for years 30–50, indicating a nonlinear response, but it does remain above that of Pac− for the entire simulation (Fig. 6c). Freshening between 30° and 50°S for Pac− is outside the range of the control between years 30 and 80. Atl− shows a freshening during the first 70 years. Other processes are likely to have influenced the ocean surface during the early years of Atl+ as the SSS between 30° and 50°S is reduced up to year 30. All of these results demonstrate that the anomalous water mass surfaces north of the Southern Ocean, as it is recirculated poleward within the subtropical gyres. Upwelling in this region is expected and has been shown using observations (e.g., Sallée et al. 2010).

As the anomalous AAIW moves into the higher latitudes (>30°), there is evidence of a SST response (Fig. 7). In the North Atlantic, surface heat flux anomalies

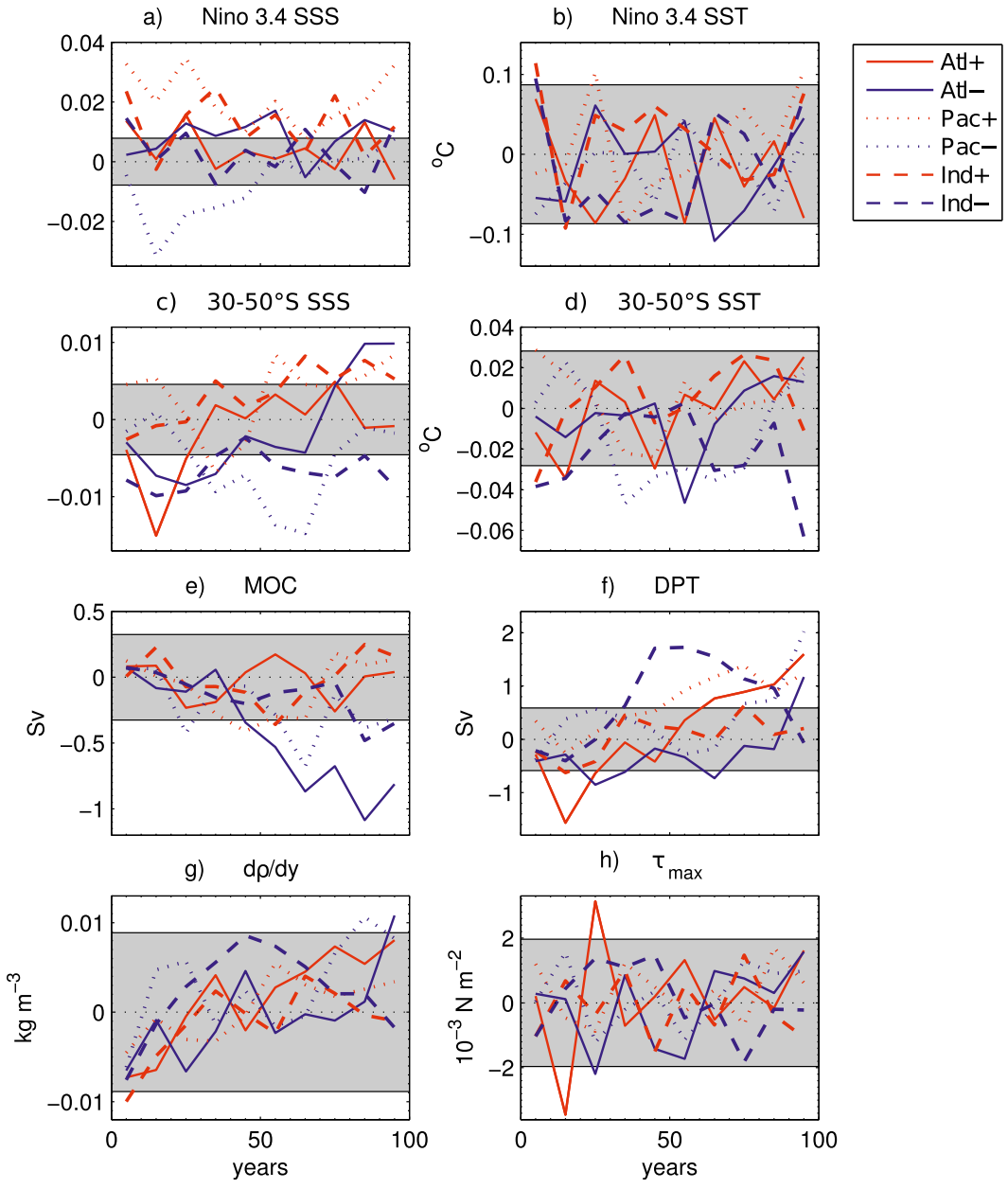

FIG. 6. Indices for Niño-3.4 (a) SSS and (b) SST (average within 5°N–5°S, 170°–120°W), zonal-mean (30°–50°S) (c) SSS and (d) SST, (e) MOC strength, (f) DPT, (g) zonal-mean meridional density gradient ($d\rho/dy$) across the SO (difference between 65° and 45°S), and (h) maximum zonal-mean wind stress τ_{max} between 30° and 70°S. Values are all ensemble-mean anomalies with respect to the 100-yr mean of the control ensemble. Blue lines show the cooling, freshening perturbations; red lines show the warming, salting perturbations. Gray shading shows the maximum range of the decadal-mean variations in the ensemble mean of the control from the 100-yr mean. Solid, dotted, and dashed lines show the Atl, Pac, and Ind experiments, respectively.

show that these SST anomalies are predominantly forced by the ocean rather than the overlying atmosphere (Fig. 10). Regions of increased SST are accompanied by negative heat flux anomalies, identifying a transfer of heat from the ocean to atmosphere, and vice versa. For Ind− and Pac−, SSS anomalies between 30° and 50°S are accompanied by SST anomalies of the same sign (Figs. 6c,d). While the responses for Ind+ and Pac+ are less consistent (and still within the range of control ensemble variability), the average temperature does remain predominantly above that of the cooling experiments (Fig. 6d). In the higher latitudes (>30°), the

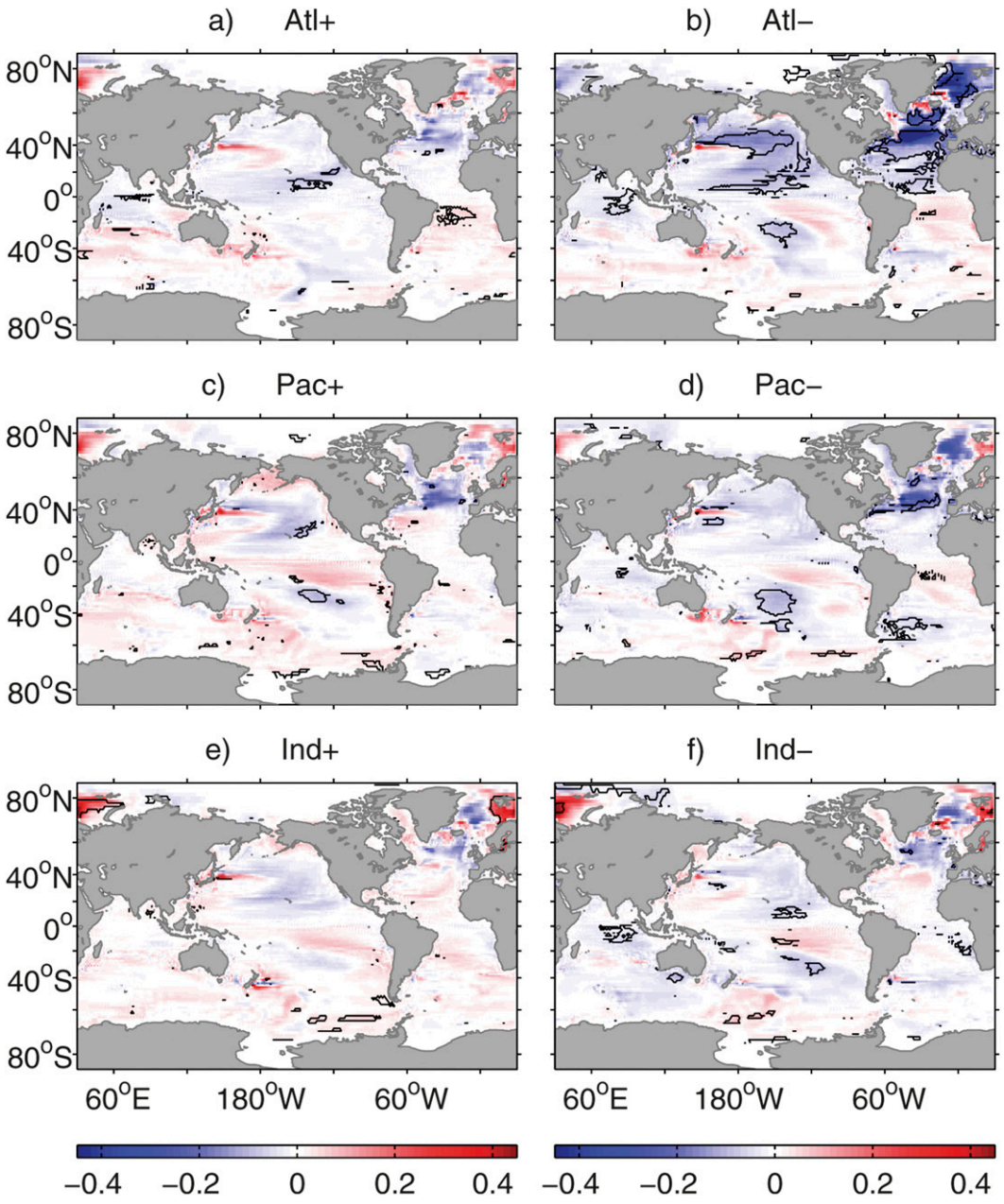

FIG. 7. Mean global SST response to each experiment for years 51–100. Values shown are anomalies with respect to the control ensemble mean for years 51–100. Black contours indicate regions where anomalies are significant at the 95% confidence level.

anomalous heat content in the surfacing water mass is then sufficient to cause a change in SST outside the range of the control ensemble. These experiments do not consider the surface ocean changes that would have necessarily occurred in AAIW formation regions, north of the Subantarctic Front. However, the results do illustrate how changes occurring in one ocean basin may spread throughout the global ocean, as the anomalous heat and salt content enters the Antarctic Circumpolar Current.

b. Changes in ocean circulation

After the water mass reaches the surface, ocean–atmosphere heat flux anomalies lead to density anomalies in the water column (Fig. 11). These density anomalies occur as the heat content changes but salinity anomalies remain (Fig. 3). Some density anomalies at intermediate depths may also result from the nonlinearity of the equation of state; however, they are smaller than

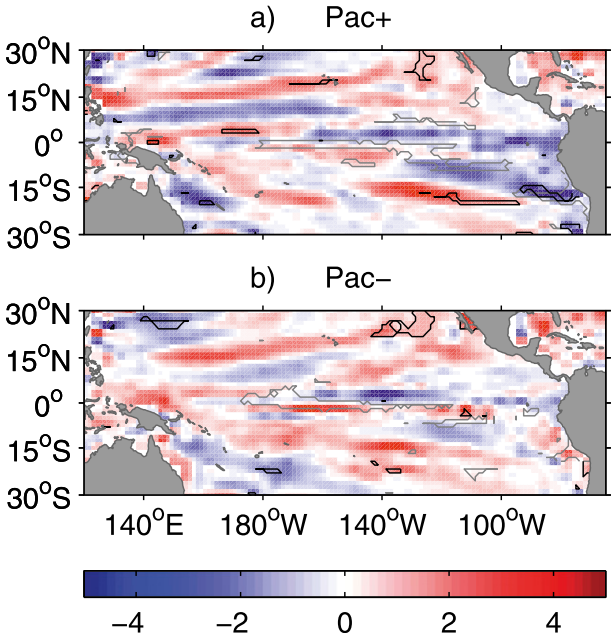

FIG. 8. Mean total net heat flux anomalies into the surface ocean for (a) Pac+ and (b) Pac− for years 1–10 (10^{-1} W m^{-2}). Values shown are anomalies with respect to the control ensemble mean for years 1–10. Positive values indicate a heat flux anomaly in the atmosphere-to-ocean direction. Black contours indicate regions where heat flux anomalies are significant at the 95% confidence level. Gray contours indicate regions where (a) positive SSS anomalies and (b) negative SSS anomalies are significant at the 95% confidence level for years 1–10.

those originating from surface heat fluxes. G11 showed that opposing density anomalies, for the warming or cooling perturbations, cause the fresher (lighter) water mass to spend a greater amount of time at shallower depths in the ocean (see their Fig. 14). The same response is also found in this study. At the end of the Atl+ simulation, 47% of the original salt perturbation remains at intermediate depths in the Atlantic (~300–1500 m), whereas for Atl−, 14% of the original salt anomaly remains at intermediate depths, with the majority residing in the upper 300 m, or sinking to deep levels in the north. These nonlinear responses can lead to changes in ocean circulation. For Atl−, the reduced density in the North Atlantic leads to a decreased MOC strength, with a reduction of more than 1 Sv (1 Sv $\equiv 10^6$ m^3 s^{-1}) after 80 years (Fig. 6e). The MOC strength is taken here to be the maximum overturning streamfunction at 45°N. The response for Atl+ is not equal in magnitude. Because the saltier water mass is denser, it spends less time at the surface, reducing the change in density within the water column, leading to little change in the MOC. Perturbations in the Pacific and Indian Oceans also lead to changes in the MOC toward the end of the simulation, as anomalous AAIW is advected into the Atlantic via Drake Passage or south of South Africa.

Changes in the meridional density gradient may also lead to nonlinear responses to warming or cooling perturbations in the Southern Ocean (SO). Here, the density of the surface layer increases toward the south, as isopycnals shoal toward the polar regions. As the cool, fresh anomalies surface north of the Antarctic Circumpolar Current (ACC), anomalous heat fluxes lead to a reduction in density (Fig. 10). This increases the meridional density gradient and hence increases the strength of the ACC. Such changes in transport can affect the global spread of the anomalous water mass. For Ind−, the volume of Drake Passage transport (DPT) is increased after 30 years (Fig. 6f), as the density difference between 65° and 45°S increases (Fig. 6g). Increased wind stress contributes to the increased DPT during years 20–50; however, negative wind stress anomalies are found after this time (Fig. 6h). Analysis of the temperature and salinity differences between 65° and 45°S shows that the increased density gradient results from freshening at 45°S. The DPT for Pac− does not increase by the same extent, but after 70 years, both the transport and meridional density gradient have increases outside the range of the control.

For the warming, salting experiments, the DPT does not show an equal and opposite response. Both Atl+ and Pac+ show an increased DPT, when compared with their opposing experiments as well as the control. The ACC is also influenced by the strength and position of the overlying westerly winds. The southern annular mode (SAM) and thus the westerly wind stress over the Southern Ocean have been shown to be influenced by the meridional SST gradient (Marshall and Connolley 2006). If warmer AAIW surfaces north of the ACC, the increased SST gradient could then alter the magnitude of the westerly wind stress. During these experiments, wind stress anomalies influence the ACC variability on interdecadal time scales (Fig. 6h). For example, the minimum in DPT for years 11–20 in Atl+ is accompanied by a negative zonal wind stress anomaly. However, there is no long-term trend in zonal wind stress or the SAM. Longer-term variability in DPT is dominated by the density anomalies in the water column rather than changes in surface temperature (Figs. 6g and 7). The positive trend seen in DPT for the majority of the experiments (Fig. 6f) occurs as a result of temperature and salinity drifts south of the ACC in the control ensemble, which act to increase the meridional density gradient.

c. *Atmospheric response*

The most significant surface air temperature (SAT) response occurs for Atl− (Fig. 12b). The direction of

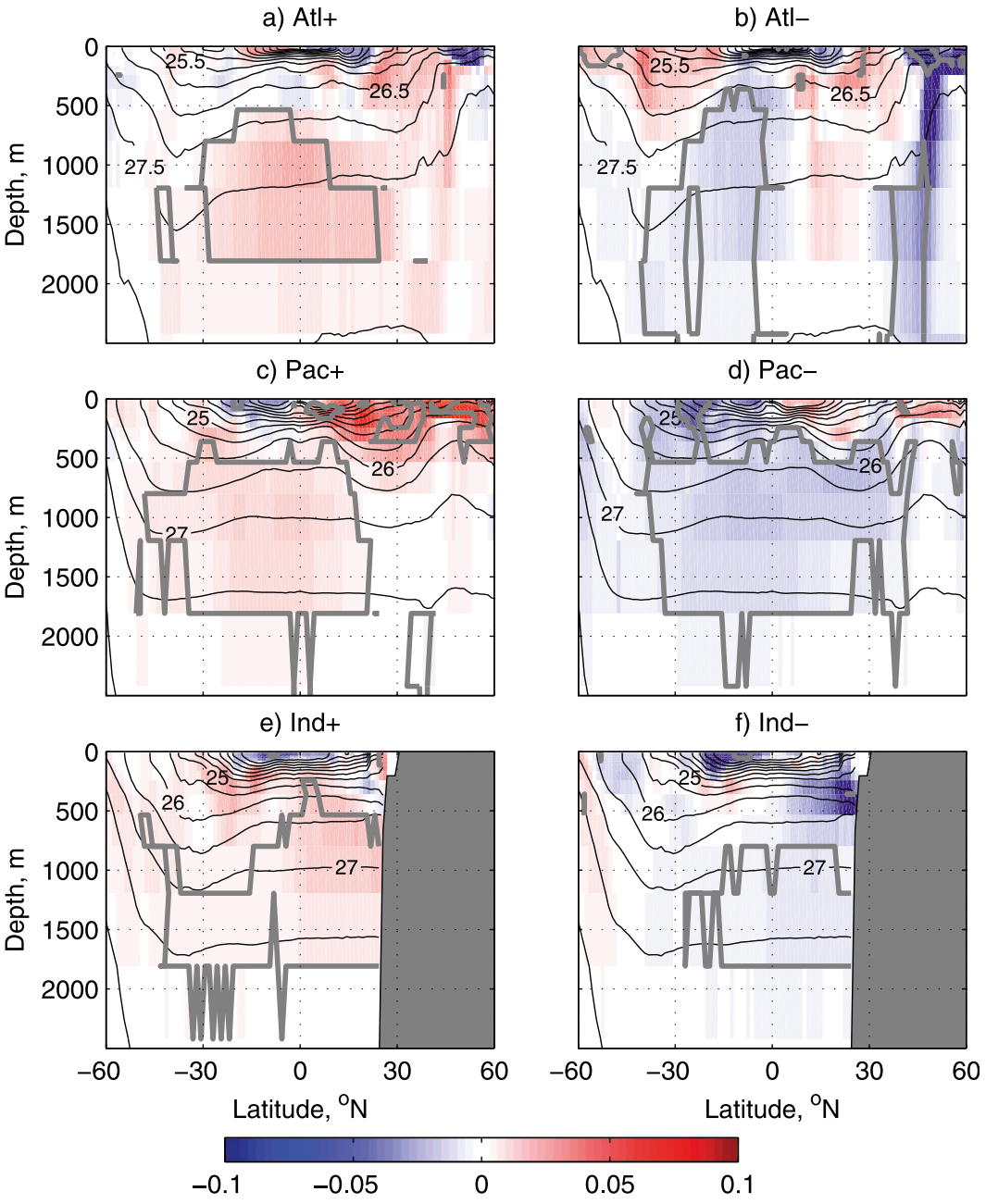

FIG. 9. Zonal average salinity anomalies for each experiment for years 91–100 with respect to the control ensemble mean for the same period. Black contours show control potential density conditions for years 91–100 relative to the surface level of HadCM3. Thick gray contours show regions where the anomalies are significant at the 95% confidence level.

surface heat flux anomalies shows that the SAT anomalies are forced by reduced SST (Fig. 10b). Reduced MOC strength (Fig. 6e), along with surfacing cooler AAIW, leads to a basinwide decrease in SST (Fig. 7b) and hence a statistically significant reduction in SAT during the latter half of the simulation. This cooling is seen throughout the Northern Hemisphere. The decreased northward ocean heat transport (OHT) also results in a warming in the South Atlantic (Fig. 7b). However, the mean SAT response over the Southern Hemisphere is not statistically significant (Fig. 12b). The relation between MOC strength, OHT, and SST in the North Atlantic, has been shown in a number of previous studies (e.g., Dong and Sutton 2002; Vellinga and Wu

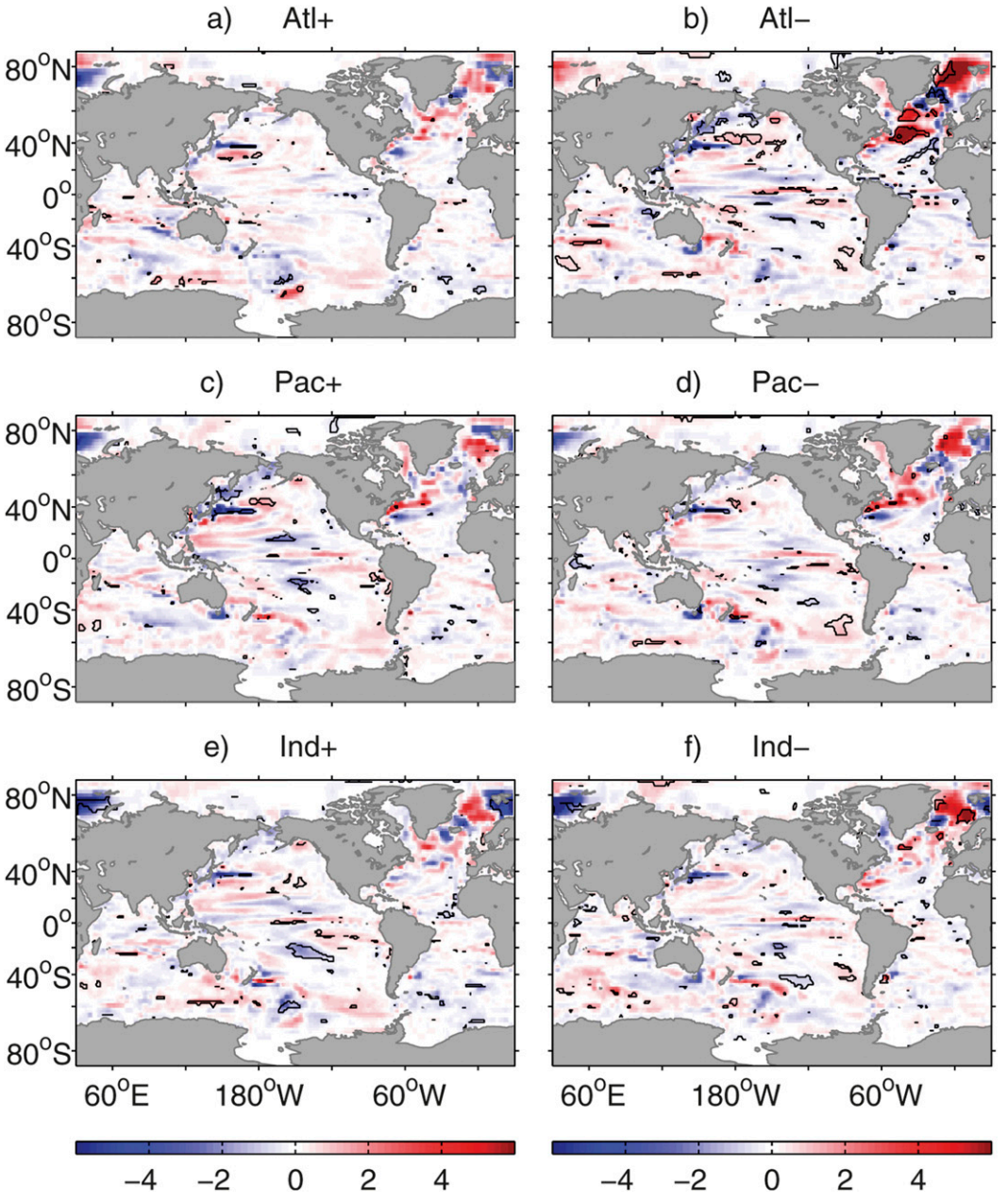

FIG. 10. Mean total net heat flux anomalies into the surface ocean for each experiment for years 51–100 (10^{-1} W m^{-2}). Values shown are anomalies with respect to the control ensemble mean for years 51–100. Positive values indicate a heat flux anomaly in the atmosphere-to-ocean direction. Black contours indicate regions where the anomalies are significant at the 95% confidence level.

2004; Knight et al. 2005). As the meridional SST gradient decreases, precipitation anomalies are found in the tropical Atlantic (Fig. 13a), consistent with a southward shift of the intertropical convergence zone (Vellinga and Wu 2004). The reduced rainfall in the North Atlantic may account for the increased salinity observed in the North Atlantic toward the end of the simulation (Fig. 9b). Previous studies have shown that basinwide changes in North Atlantic SST can lead to mean sea level pressure (MSLP) and precipitation anomalies over the surrounding continents (Sutton and Hodson 2005). However, despite the strong cooling evident during Atl−, there is no significant response in MSLP or precipitation over North America, Europe, or Africa (Fig. 13).

The response over the Atlantic and surrounding continents during Atl+ is less than that seen in Atl− (Fig. 12a).

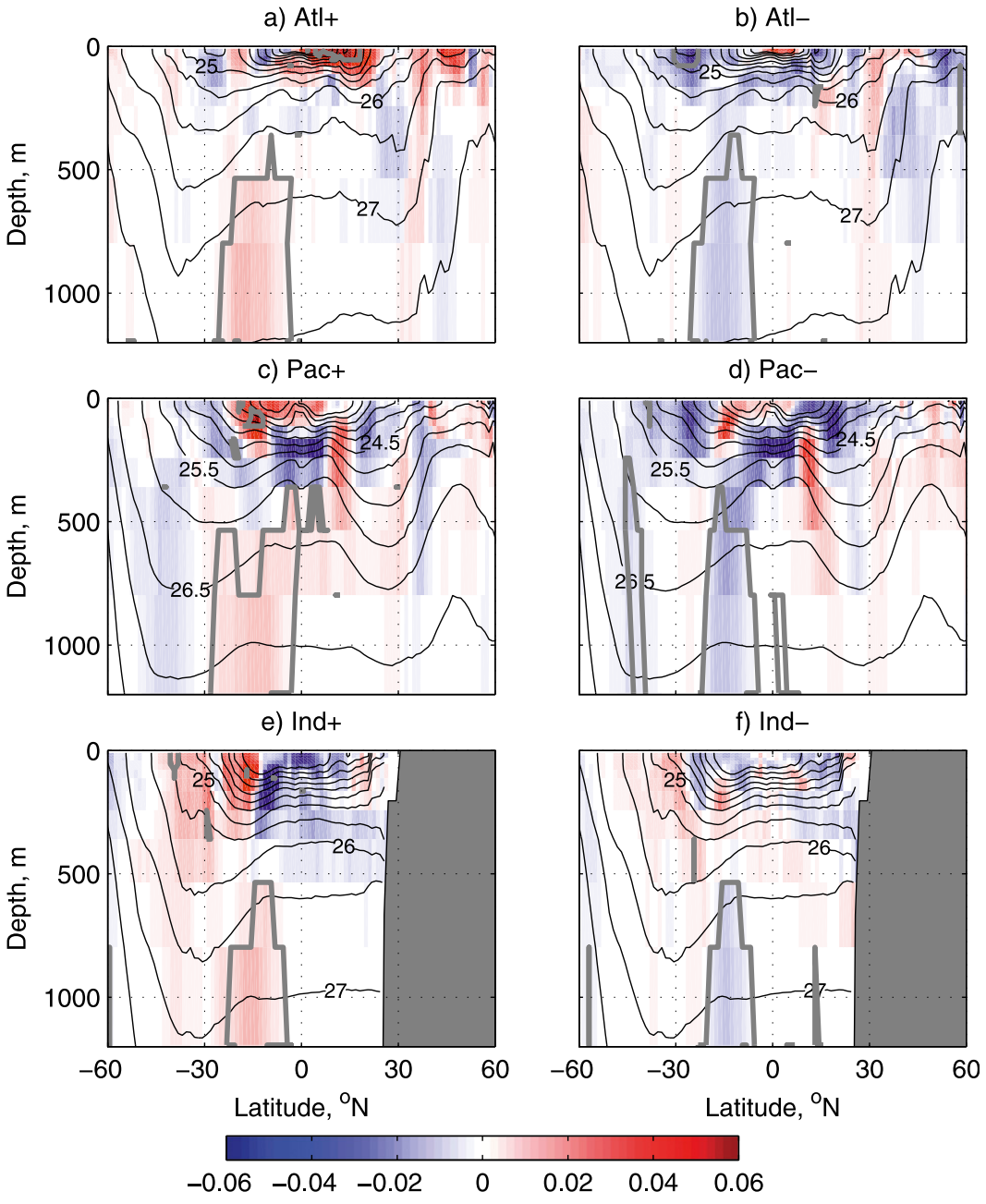

FIG. 11. Zonal average density anomalies for each experiment for years 1–10 with respect to the control ensemble mean for the same period. Black contours show control potential density conditions for years 1–10 relative to the surface level of HadCM3. Thick gray contours show regions where the anomalies are significant at the 95% confidence level.

The anomalous water mass spends less time at the surface, and there is no significant increase in MOC strength to increase the meridional OHT (Fig. 6e). However, increased SAT can be found around the tip of Greenland and in the Greenland–Iceland–Norwegian (GIN) Seas, corresponding to regions of increased SST and SSS (Figs. 5a, 7a, and 12a).

For perturbations in the Pacific and Indian Oceans, the spatial patterns of SAT anomalies over the Atlantic are similar to those seen for the Atlantic experiments (Fig. 12). The response in the Atlantic MOC is similar (Fig. 6e), although the magnitude is influenced by the volume of anomalous AAIW entering the basin. Both Pac− and Ind− have a decreased MOC strength, which

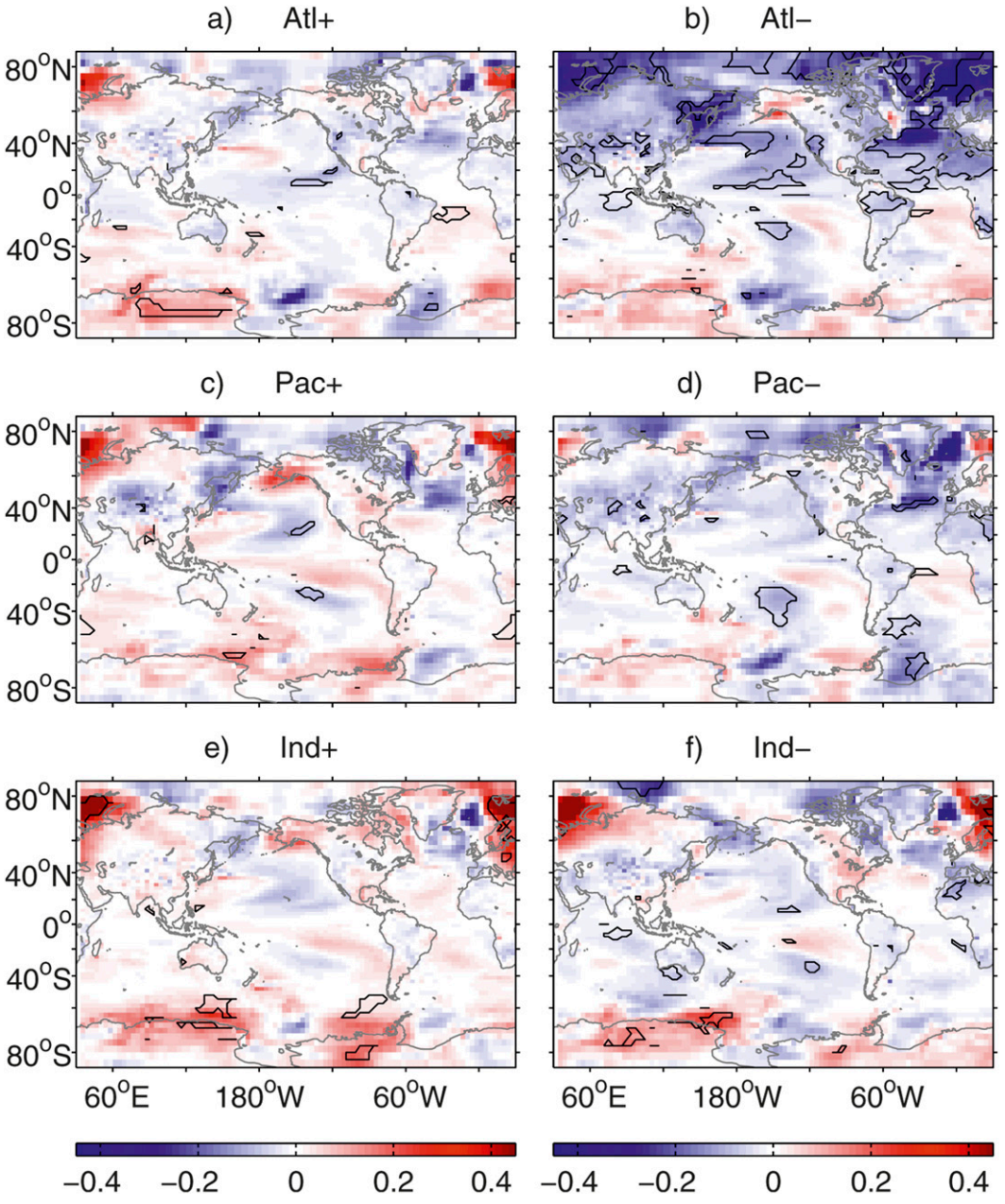

FIG. 12. Mean global SAT response to each experiment for years 51–100. Values shown are anomalies with respect to the control ensemble mean for years 51–100. Black contours indicate regions where the anomalies are significant at the 95% confidence level.

is outside the range of the control. This leads to a cooling of the North Atlantic in the latter half of the simulation (Figs. 12d,f). For Ind+, the MOC strength increases during years 80–100, contributing to a more significant warming in the North Atlantic than that seen for Atl+ and Pac+ (Figs. 12a,c,e). For the regions surrounding the Barents Sea, a reduction in sea ice cover during years 81–90 is the likely cause of significant warming. The sea ice cover in this region is thin, making the region sensitive to increases in ocean heat transport.

For Atl− there is a strong cooling over the North Atlantic Current (NAC; Fig. 12b). These SAT anomalies are forced by reduced SST in the NAC (Figs. 7a,b and 10) and are not caused by a southward expansion of the subpolar gyre (SPG). G11 show that a persistent cooling in the NAC, lasting from year 30 to the end of

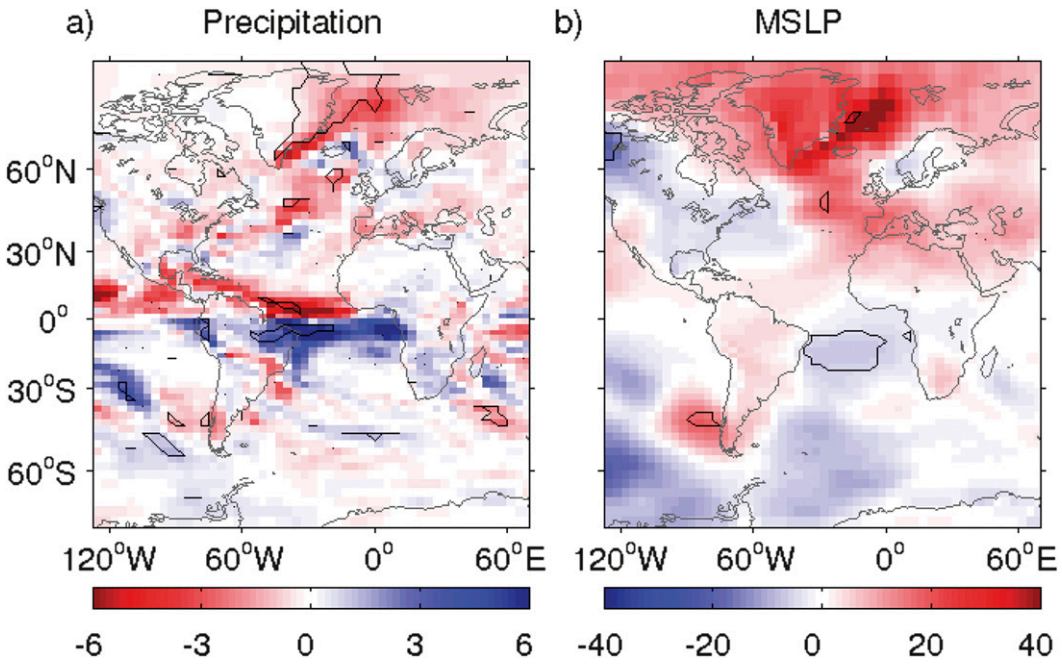

FIG. 13. Mean atmospheric anomalies for Atl− for years 51–100: (a) precipitation (cm yr^{-1}) and (b) MSLP (Pa). Values shown are anomalies with respect to the control ensemble mean for years 51–100. Black contours indicate regions where the anomalies are significant at the 95% confidence level.

the simulation, results from a divergence of OHT, with an increased SPG transport bringing cooler, fresher water into the NAC. For Atl−, the cooling is less persistent, lasting from year 60 to the end of the simulation. G11 show that cooler AAIW surfaces in the NAC as it is advected northward. The reduced SST forces an increased MSLP over the region, causing wind stress anomalies that act to strengthen the SPG. As the increased SPG transport then brings cooler, fresher water into the NAC, this leads to a significant response to the initial perturbation. For Atl−, cooling occurs over a larger area of the North Atlantic than observed in G11. This leads to a larger area of increased MSLP over the GIN seas and subtropical North Atlantic during years 51–100 (Fig. 13b). The resulting difference in wind stress anomalies over the SPG may account for the difference in persistence of cold anomalies in the NAC between Atl− and previous experiments (G11).

For Atl+, cool anomalies are also found in the NAC, although they are less persistent than those seen for Atl−, lasting up to 20 years. This cooling in the NAC for Atl+ follows periods of increased convection in the Labrador Sea and hence increased Labrador Sea Water production. As the remnants of warmer AAIW arrive in the SPG and GIN Seas, increased SST leads to reduced MSLP over Greenland and the GIN Seas, as shown in Fig. 14 for years 31–40. These low pressure anomalies lead to increased wind stress over the Labrador Sea and deeper surface mixed layers. Wind stress anomalies over the SPG also increase the transport of cooler, fresher water southward, into the NAC. However, this is not the sole mechanism for the cold anomalies during the 100-yr simulation. SST variability is also influenced by natural variability associated with the North Atlantic Oscillation. For Atl+, the average reduction in SST and SAT is not significant over years 51–100 (Figs. 7a and 12a). Similar responses to those seen in the Atlantic experiments can also be seen over the NAC for the Pacific and Indian experiments (Figs. 12c–f).

As the anomalies surface north of the Southern Ocean (between 30° and 50°S), SAT anomalies occur for both the warming and cooling experiments (Fig. 12). The response is most apparent in the southern Indian Ocean for Ind+ and Ind−, because of the net southward transport of anomalous intermediate waters in the Indian Ocean (You 1998; Banks 2000a). For Ind−, the SAT anomalies extend into both the Pacific and Atlantic Oceans (Fig. 12f). As the ACC transport increases, this allows the cooler AAIW to spread eastward into the Pacific. Transport of anomalies into the Atlantic is expected in the Agulhas Current. The representation of the Agulhas Current and retroflection in HadCM3 is poor, leading to larger volumes of AAIW entering the Atlantic through this route than would be seen in reality (Banks 2000b). However, this path of AAIW transport is consistent with both previous modeling studies and observations (e.g.,

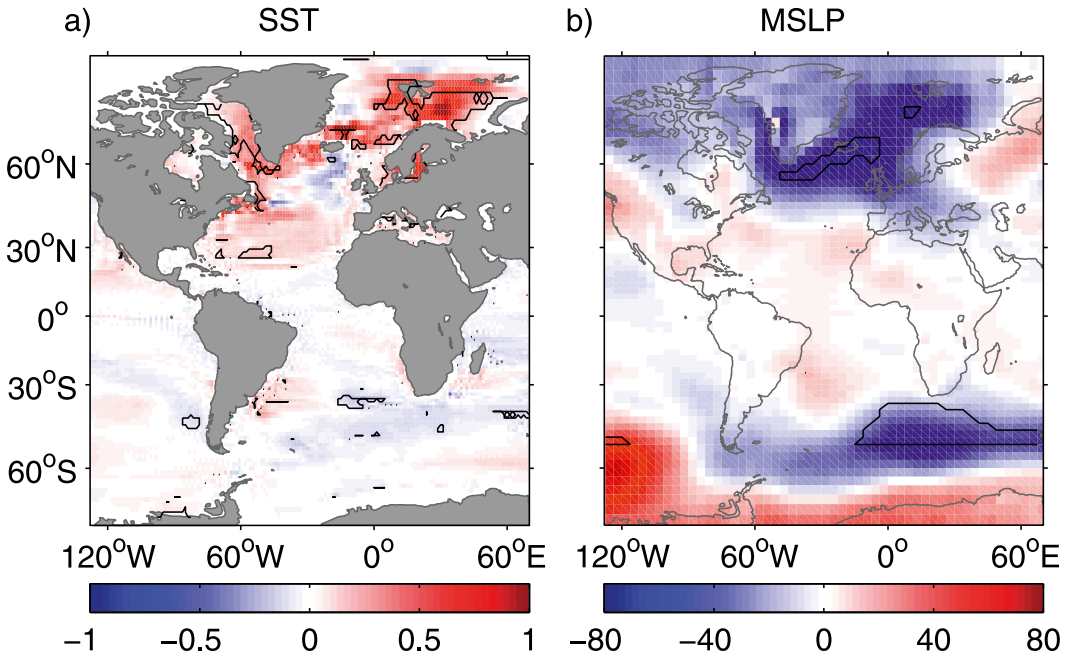

FIG. 14. Mean surface anomalies for Atl+ for years 31–40: (a) SST (°C) and (b) MSLP (Pa). Values shown are anomalies with respect to the control ensemble mean for years 31–40. Black contours indicate regions where the anomalies are significant at the 95% confidence level.

Sen Gupta and England 2007; McCarthy et al. 2011). SST anomalies in the Southern Ocean have previously been shown to cause shifts in the SAM (Marshall and Connolley 2006); however, there were few significant anomalies and no long-term trends in MSLP or the SAM over the Southern Ocean in any of these experiments. Farther south, SAT anomalies are found around Antarctica (Fig. 12). As with the Barents Sea, the region west of the Antarctic Peninsula experiences greater warming as the sea ice cover decreases. Significant warming west of the Peninsula is found for the case of Ind+. However, as every experiment experiences a warming, for both warming and cooling initial perturbations, it is unclear whether these results are a true response to changes in AAIW. Instead, these anomalies may be due to internal variability of the control climate system.

Over the Pacific Ocean, SST and SAT anomalies predominantly resemble the Pacific decadal oscillation (PDO) (Mantua et al. 1997; Figs. 7 and 12). Previous studies have shown that such variability is linked with SST in the tropical Pacific and is likely due to El Niño–Southern Oscillation variability, along with the reemergence of SST anomalies from previous winters (Collins et al. 2001; Newman et al. 2003). For each of the perturbations, the PDO is observed in the same phase during the latter half of the experiment. Also, SST anomalies in this region do not typically coincide with SSS anomalies of the same sign (Figs. 7 and 5). Therefore, it is likely that the temperature anomalies seen in the North Pacific for Pac+ and Pac− are influenced by internal variability in the model and are not a result of these perturbations.

4. Discussion and conclusions

The aim of this study has been to demonstrate the global impact of changes in AAIW. Although perturbations were made in each ocean basin separately, a comparison of these results enables us to determine the potential response to changes on a global scale. The results from this series of experiments are summarized in Fig. 15. The key regions where AAIW is found to reach the surface are either in the equatorial or coastal regions, where the prevailing winds lead to divergent Ekman transport and upwelling, or at mid- to high latitudes (>30°), where isopycnals shoal toward the surface, and deeper mixed layers can bring anomalies to the surface. Although SSS anomalies are found in each of these regions, they are not always accompanied by surface temperature anomalies, as heat can be transferred rapidly between the ocean and atmosphere. After the anomalous water mass reaches the surface, resultant ocean–atmosphere heat fluxes can then cause a nonlinear response to opposite perturbations.

In the equatorial regions, there is an approximately linear response, as both the warmer and cooler AAIW

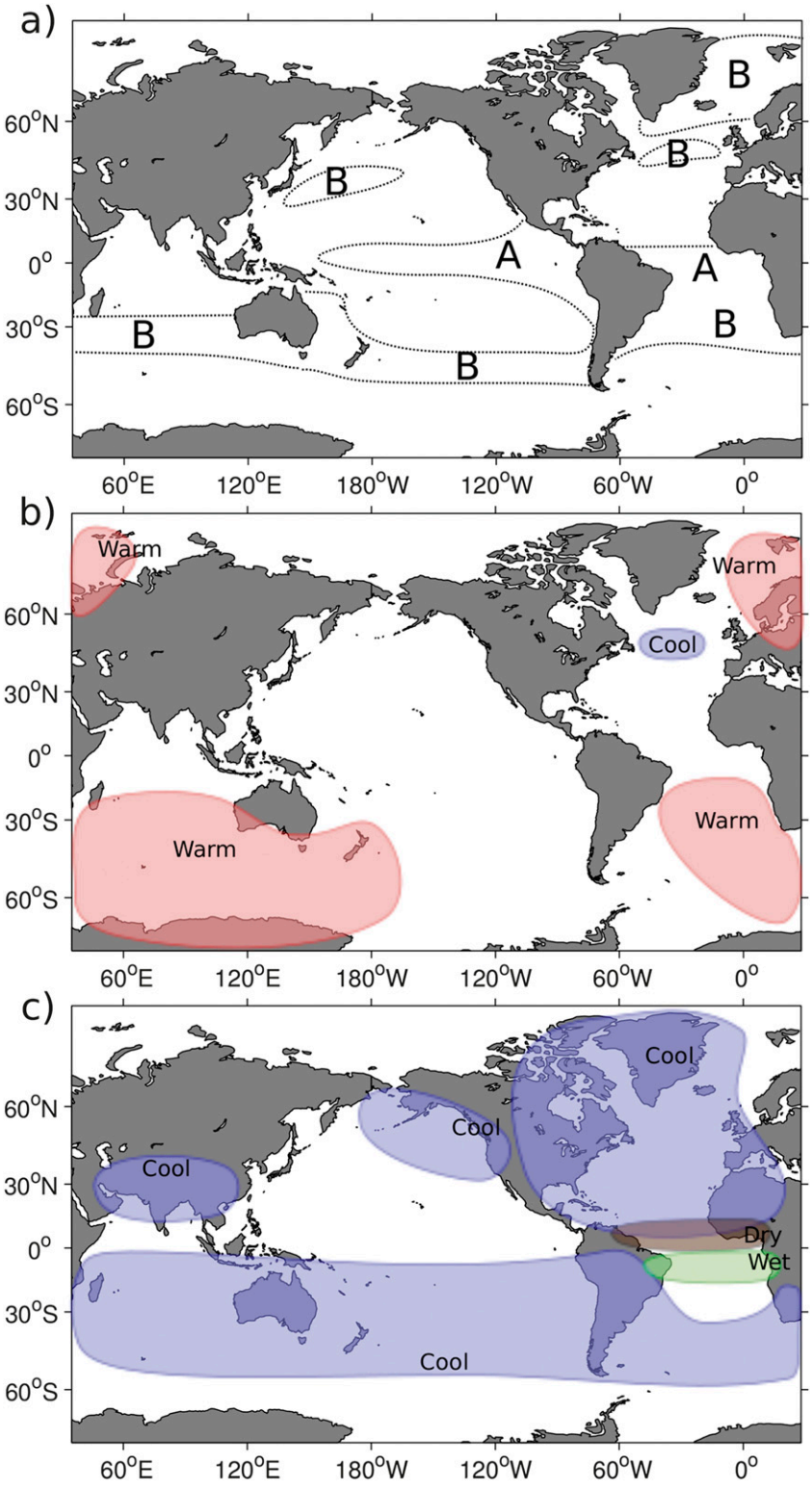

FIG. 15. Schematics to summarize the response to AAIW perturbations. (a) Regions where AAIW reaches the surface: A—through equatorial or coastal upwelling; B—due to shoaling isopycnals and deeper mixed layers. The atmospheric response to (b) warming (Atl+, Pac+, Ind+) and (c) cooling (Atl−, Pac−, Ind−) perturbations. The responses shown here on the global scale have been subjectively determined by comparing significant results from the Atl, Pac, and Ind experiments.

surfaces in this region. However, after the perturbed water mass reaches the surface, ocean–atmosphere heat fluxes result in density anomalies. These density anomalies cause significant changes in ocean circulation, such as MOC strength and ACC transport. For example, the strength of the Atlantic MOC decreases during Atl−, but there is no significant change for Atl+. This response to a warm, salty anomaly in Atlantic Intermediate Waters was unexpected and contrary to that presented in a previous study (Banks et al. 2007). In a different climate model, Banks et al. (2007) showed that as Atlantic AAIW was replaced by a warm, salty intermediate water, the MOC strength increased. However, it is worth noting that the temperature and salinity anomalies in the Banks et al. (2007) study were greater than those in Atl+, with mean anomalies of up to 1°C in temperature and 0.2 in salinity, extending throughout the Atlantic (north of 30°S) at intermediate depths. The response in Atl+ also differs from that presented by G11, where the warming, salting experiment showed similar results to the cooling, freshening experiment, including a decline in the MOC strength. The responses presented in G11 are influenced by the initial ocean state used for the ensemble simulation. The MOC response in Atl− is greater and more significant than the response to cooler, fresher AAIW shown by G11.

The combination of various nonlinear responses in the ocean means that the cooler, fresher perturbations have a greater impact on the atmosphere than the warmer, saltier perturbations (Figs. 15b,c). The greatest impacts occur when the surfacing anomaly leads to a change in ocean circulation that acts to strengthen the original heat anomaly. This may happen as the density anomalies allow the water mass to spend a greater time at the surface, or as the OHT into the region is changed. The atmospheric response to SST anomalies (MSLP and wind stress) can also influence the ocean circulation and heat transport. All of these effects result in the North Atlantic being surprisingly sensitive to cool, fresh anomalies in AAIW, and the global SAT response for Atl− being more significant than for any of the other perturbations (Figs. 12 and 15).

Future climate projections suggest that the region surrounding the North Atlantic is likely to experience a slower rate of warming, when compared with other regions of the Northern Hemisphere, because of a reduced MOC strength (Meehl et al. 2007). A multimodel ensemble showed an average reduction of 25% by 2099 under increasing CO_2 emissions. While the aim of this idealized study has been to identify mechanisms rather than to make predictions of the magnitude of future changes, the 5% reduction in MOC strength during the Atl− experiment suggests that a cooler, fresher AAIW would contribute to a reduced rate of warming in the North Atlantic region.

Previous studies have shown that the core of AAIW may become warmer and fresher under a warming climate, resulting in a lighter water mass (Sen Gupta et al. 2009; Downes et al. 2010). Although this study necessitated the use of density-compensating perturbations, in order to maintain the same initial paths of circulation, it is possible to use the results presented here to consider the impact of warmer, fresher AAIW. First, as the lighter water mass may move northward at shallower depths, this would allow greater contact with the upper ocean and surface mixed layer. The results from these experiments suggest that the heat released to the overlying atmosphere at low latitudes would not have a significant impact on the climate system. However, if a lighter AAIW reaches the North Atlantic, it would likely contribute to a decreased MOC. The resultant cooling in the North Atlantic would depend on the relative impact of the reduced MOC, compared with the increased heat content of the intermediate water mass. Downes et al. (2010) also show that the subduction rate of AAIW is likely to decrease, because of increased buoyancy in the surface formation regions, along with decreased mixed-layer depths. As the volume of AAIW moving northward through the ocean decreases, reducing the meridional heat and freshwater transport, this may alter the response in the Northern Hemisphere. Further work is needed to understand the relative importance of each of these potential changes on the climate system.

Despite a range in strength and significance, each experiment from this study shows a response to AAIW change, in both the ocean and atmosphere. Following perturbations between 10° and 20°S, SST responses can occur within 10 years and illustrate the importance of AAIW properties for decadal forecasting systems. Responses in the Atlantic MOC occur on time scales longer than 50 years and demonstrate that there is a need to monitor intermediate waters and their variability in order to fully understand how our climate will change under future emissions scenarios. These experiments show that there is not a simple, linear response to changes at intermediate depths. The response to a cooler, fresher AAIW is the greatest and most significant.

Acknowledgments. Funding has been provided by a Ph.D. studentship for the U.K. Natural Environment Research Council and a CASE studentship with the British Antarctic Survey. The research presented in this paper was carried out on the High Performance Computing Cluster supported by the Research Computing Service at the University of East Anglia. We thank

Ian Stevens for his technical support in the initial stages of this project.

REFERENCES

Aoki, S., N. L. Bindoff, and J. A. Church, 2005: Interdecadal water mass changes in the Southern Ocean between 30°E and 160°E. *Geophys. Res. Lett.,* **32,** L07607, doi:10.1029/2004GL022220.

Banks, H. T., 2000a: Indonesian Throughflow in a coupled climate model and the sensitivity of the heat budget and deep overturning. *J. Geophys. Res.,* **105** (C11), 26 135–26 150.

——, 2000b: Ocean heat transport in the South Atlantic in a coupled climate model. *J. Geophys. Res.,* **105** (C1), 1071–1092.

——, and N. L. Bindoff, 2003: Comparison of observed temperature and salinity changes in the Indo-Pacific with results from the coupled climate model HadCM3: Processes and mechanisms. *J. Climate,* **16,** 156–166.

——, S. Stark, and A. B. Keen, 2007: The adjustment of the coupled climate model HadGEM1 toward equilibrium and the impact on global climate. *J. Climate,* **20,** 5815–5826.

Bindoff, N. L., and T. J. McDougall, 2000: Decadal changes along an Indian Ocean section at 32°S and their interpretation. *J. Phys. Oceanogr.,* **30,** 1207–1222.

Collins, M., S. F. B. Tett, and C. Cooper, 2001: The internal climate variability of HadCM3, a version of the Hadley Centre coupled model without flux adjustments. *Climate Dyn.,* **17,** 61–81.

Dong, B., and R. T. Sutton, 2002: Variability in North Atlantic heat content and heat transport in a coupled ocean–atmosphere GCM. *Climate Dyn.,* **19** (5–6), 485–497.

Downes, S. M., N. L. Bindoff, and S. R. Rintoul, 2010: Changes in the subduction of Southern Ocean water masses at the end of the twenty-first century in eight IPCC models. *J. Climate,* **23,** 6526–6541.

Gordon, C., C. Cooper, C. A. Senior, H. Banks, J. M. Gregory, T. C. Johns, J. F. B. Mitchell, and R. A. Wood, 2000: The simulation of SST, sea ice extents and ocean heat transports in a version of the Hadley Centre coupled model without flux adjustments. *Climate Dyn.,* **16** (2–3), 147–168, doi:10.1007/s003820050010.

Graham, J. A., D. P. Stevens, K. J. Heywood, and Z. Wang, 2011: North Atlantic climate responses to perturbations in Antarctic Intermediate Water. *Climate Dyn.,* **37,** 297–311, doi:10.1007/s00382-010-0981-1.

Hanawa, K., and L. D. Talley, 2001: Mode waters. *Ocean Circulation and Climate,* G. Siedler, J. Church, and J. Gould, Eds., Academic Press, 373–386.

Helm, K. P., N. L. Bindoff, and J. A. Church, 2010: Changes in the global hydrological-cycle inferred from ocean salinity. *Geophys. Res. Lett.,* **37,** L18701, doi:10.1029/2010GL044222.

Knight, J. R., R. J. Allan, C. K. Folland, M. Vellinga, and M. E. Mann, 2005: A signature of persistent natural thermohaline circulation cycles in observed climate. *Geophys. Res. Lett.,* **32,** L20708, doi:10.1029/2005GL024233.

Mantua, N., S. Hare, Y. Zhang, J. Wallace, and R. Francis, 1997: A Pacific interdecadal climate oscillation with impacts on salmon production. *Bull. Amer. Meteor. Soc.,* **78,** 1069–1079.

Marshall, D., 1997: Subduction of water masses in an eddying ocean. *J. Mar. Res.,* **55,** 201–222.

Marshall, G. J., and W. M. Connolley, 2006: Effect of changing Southern Hemisphere winter sea surface temperatures on southern annular mode strength. *Geophys. Res. Lett.,* **33,** L17717, doi:10.1029/2006GL026627.

McCarthy, G., E. McDonagh, and B. King, 2011: Decadal variability of thermocline and intermediate waters at 24°S in the South Atlantic. *J. Phys. Oceanogr.,* **41,** 157–165.

McCartney, M. S., 1977: Subantarctic Mode Water. *Deep-Sea Res.,* **24** (Suppl.), 103–119.

Meehl, G. A., and Coauthors, 2007: Global climate projections. *Climate Change 2007: The Physical Science Basis,* S. Solomon et al., Eds., Cambridge University Press, 747–845.

Molinelli, E., 1981: The Antarctic influence on Antarctic Intermediate Water. *J. Mar. Res.,* **39,** 267–293.

Naveira Garabato, A. C., L. Jullion, D. P. Stevens, K. J. Heywood, and B. A. King, 2009: Variability of Subantarctic Mode Water and Antarctic Intermediate Water in the Drake Passage during the late twentieth and early twenty-first centuries. *J. Climate,* **22,** 3661–3688.

Newman, M., G. Compo, and M. Alexander, 2003: ENSO-forced variability of the Pacific decadal oscillation. *J. Climate,* **16,** 3853–3857.

Oke, P., and M. England, 2004: Oceanic response to changes in the latitude of the Southern Hemisphere subpolar westerly winds. *J. Climate,* **17,** 1040–1054.

Pardaens, A. K., H. T. Banks, J. M. Gregory, and P. R. Rowntree, 2003: Freshwater transports in HadCM3. *Climate Dyn.,* **21,** 177–195.

Piola, A. R., and A. L. Gordon, 1989: Intermediate waters in the southwest South Atlantic. *Deep-Sea Res.,* **36,** 1–16.

Sallée, J.-B., K. Speer, S. Rintoul, and S. Wijffels, 2010: Southern Ocean thermocline ventilation. *J. Phys. Oceanogr.,* **40,** 509–529.

Santoso, A., and M. H. England, 2004: Antarctic Intermediate Water circulation and variability in a coupled climate model. *J. Phys. Oceanogr.,* **34,** 2160–2179.

Schmidtko, S., and G. C. Johnson, 2012: Multi-decadal warming and shoaling of Antarctic Intermediate Water. *J. Climate,* **25,** 207–221.

Sen Gupta, A., and M. H. England, 2007: Evaluation of interior circulation in a high-resolution global ocean model. Part II: Southern Hemisphere intermediate, mode, and thermocline waters. *J. Phys. Oceanogr.,* **37,** 2612–2636.

——, A. Santoso, A. S. Taschetto, C. C. Ummenhofer, J. Trevena, and M. H. England, 2009: Projected changes to the Southern Hemisphere ocean and sea ice in the IPCC AR4 climate models. *J. Climate,* **22,** 3047–3078.

Sloyan, B. M., and I. V. Kamenkovich, 2007: Simulation of Subantarctic Mode and Antarctic Intermediate Waters in climate models. *J. Climate,* **20,** 5061–5080.

——, L. D. Talley, T. K. Chereskin, R. Fine, and J. Holte, 2010: Antarctic Intermediate Water and Subantarctic Mode Water formation in the southeast Pacific: The role of turbulent mixing. *J. Phys. Oceanogr.,* **40,** 1558–1574.

Sutton, R. T., and D. L. R. Hodson, 2005: Atlantic Ocean forcing of North American and European summer climate. *Science,* **309,** 115–118.

Talley, L. D., 1996: Antarctic Intermediate Water in the South Atlantic. *South Atlantic—Present and Past Circulation,* G. Wefer et al., Eds., Springer-Verlag, 219–238.

Vellinga, M., and P. L. Wu, 2004: Low-latitude freshwater influence on centennial variability of the Atlantic thermohaline circulation. *J. Climate,* **17,** 4498–4511.

Wong, A. P. S., N. L. Bindoff, and J. A. Church, 1999: Large-scale freshening of intermediate waters in the Pacific and Indian Oceans. *Nature,* **400,** 440–443.

You, Y., 1998: Intermediate water circulation and ventilation of the Indian Ocean derived from water-mass contributions. *J. Mar. Res.,* **56,** 1029–1067, doi:10.1357/002224098765173455.